Mt-UcGAN: Multi-task uncertainty-constrained GAN for joint segmentation, quantification and uncertainty estimation of renal tumors on CT

Yanan Ruan[1], Dengwang Li[1*], Harry Marshall[2], Timothy Miao[3], Tyler Cossetto[3], Ian Chan[3], Omar Daher[3], Fabio Accorsi[3], Aashish Goela[3], and Shuo Li[4*]

[1] Shandong Key Laboratory of Medical Physics and Image Processing, Shandong Institute of Industrial Technology for Health Sciences and Precision Medicine, School of Physics and Electronics, Shandong Normal University, Jinan, Shandong 250358, China

[2] Department of Radiology, David Geffen School of Medicine at the University of California, Los Angeles, CA 90095, USA

[3] Department of Medical Imaging, Western University Schulich School of Medicine and Dentistry, London ON, Canada

[4] University of Western Ontario, London ON, Canada

Abstract. The segmentation of renal tumor, quantification of tumor indices (i.e., the center point coordinates, diameter, circumference, and cross-sectional area) and uncertainty estimation of segmentation are the key processes for clinical tumor disease diagnosis. However, these tasks have been studied independently so far. Because segmentation and quantification tasks have different optimization types, representing two different tasks as a unified optimization framework is a severe challenge. In this paper, we propose a unified framework (i.e., Mt-UcGAN: multi-task uncertainty-constrained generative adversarial network) for joint segmentation, quantification, and uncertainty estimation of renal tumors on CT. Mt-UcGAN includes a multitasking integrated generator (MtIG) and an uncertainty-constrained discriminator (UcD). MtIG achieves multi-task joint learning by novelly merging skip connections and Monte Carlo sampling. UCD guides the learning of segmentation and quantification networks by innovatively feeding prior information with high uncertainty constraints. Mt-UcGAN effectively corrects tumor prediction errors and improves network performance through continuous adversarial learning and alternate training. Experiments are performed on CT of 113 renal tumor patients. The dice coefficient of Mt-UcGAN is 92.1%, and the R^2 coefficient of tumor circumference is 0.9513. The results show that this method has great potential to be extended to other medical image analysis tasks and clinical application value.

Keywords: Segmentation · Quantification · Uncertainty estimation.

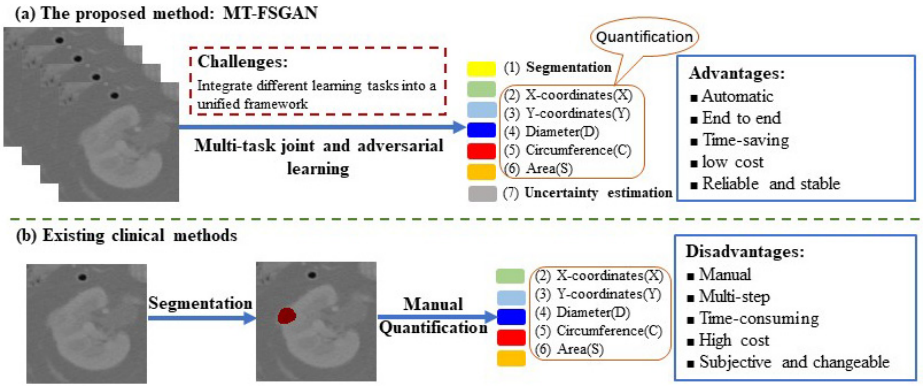

Fig. 1. (a) Our method simultaneously implements pixel-level semantic segmentation, quantification of five tumor indices (tumor diameter(D), circumference(C), cross-sectional area(S), and center point coordinates(X, Y)) and uncertainty estimation through joint learning and adversarial learning, which are time-saving, end-to-end, reliable and stable. (b)The existing clinical method is to segment through algorithm first and then the doctors manual quantify by visual observation and experience, which is time-consuming, multi-step, subjective and changeable because quantification accuracy depends on segmentation accuracy. And so far there has been no research on uncertainty estimation.

1 Introduction

The segmentation, quantification, and uncertainty estimation of renal tumors on CT images are key processes in clinical tumor disease diagnosis. Some important renal tumor indices, such as tumor diameter, perimeter, cross-sectional area, and center point coordinates, are an important basis for tumor diagnosis [1, 2]. Therefore, accurate quantification of the tumor indices is essential for accurate diagnosis of tumors. However, manual segmentation and quantification are challenging and time-consuming in practice and show high intra- and inter-operator variability [3]. The advantage of the renal tumor segmentation method is that it can provide physicians with visual inspection and pixel-level semantic interpretation based on the segmentation results [4–7]. However, due to the need for additional geometric calculations, the final quantification result of tumor indices is usually affected by the segmentation accuracy.

Direct quantification methods of tumor indices cannot provide a visual examination and pixel-level semantic interpretation for clinicians, which limits the potential clinical use of this method [8]. So far, the two tasks of segmentation and quantification have been studied independently [9–15]. The segmentation task is a discrete pixel-level classification problem, while direct exponential quantification is a global regression problem. These two tasks have different optimization types. Therefore, representing two different tasks as a unified optimization framework is a serious challenge. However, these two tasks are common in nature and have a strong complementary relationship [16–18]. By modeling these two tasks

into a unified framework, joint and efficient optimization can be achieved, and the performance of automatic quantification of tumor indices can be improved.

Uncertainty is the feedback of clinical diagnosis. Specifically, uncertainty estimation can avoid overconfidence and erroneous quantification, and allow clinicians to further modify cases with higher uncertainty [19–21]. And it can also provide clinicians with feedback on the reliability of the results, which helps doctors to conduct subsequent visual inspections and revisions on the results to further improve the accuracy of the diagnosis. This is crucial for clinical diagnosis, especially with the popularization of automatic tumor segmentation algorithms. More importantly, uncertainty estimation can feed important prior information to deep learning networks to guide the learning of the network. However, current research on renal tumors ignores this vital task.

In this paper, the multi-task uncertainty-constrained generative adversarial network (Mt-UcGAN) is proposed for joint segmentation, quantification, and uncertainty estimation of renal tumors. We creatively proposed an adversarial mechanism with uncertainty constraints, consisting of two competing modules: 1) Multitasking integrated generator, which novelly integrates skip connections to force the integration of segmentation and quantification tasks that share the same encoder into a unified optimization framework, thereby learning the shared representation of segmentation and quantification to generate beneficial interactions. 2) Uncertainty-constrained discriminator, which creatively feeds prior knowledge of the prediction result with high uncertainty to the generator, and guides the learning of segmentation and quantification networks through a multi-task comprehensive loss function.

Our contributions are: 1) For the first time, a unified framework for joint segmentation, quantification, and uncertainty estimation of renal tumors was proposed. It provides clinicians with direct assessment of the clinically necessary indicators of renal tumors while segmenting tumors, and the reliability of segmentation. 2) A novel multitasking integrated generator is proposed, which incorporates skip connections to effectively reduce the interference of unified optimization of segmentation and quantification on segmentation. 3) An innovative uncertainty-constrained adversarial mechanism is proposed, which effectively feedbacks the prior knowledge of high uncertainty constraints to guide the learning of segmentation and quantification networks.

2 Methodology

Our Mt-UcGAN simultaneously segments and quantifies renal tumors, and estimates the uncertainty of the segmentation results through multi-task uncertainty-constrained GAN mechanism (see Fig. 2). It is implemented through two collaborative modules: 1) Multitasking integrated generator (Sect. 2.1) consists of a region of interest extractor (see Fig. 2(a)) for the extraction of tumor regions of interest to reduce the input noise and the post-processing amount of data, an encoder-decoder with MC-dropout (see Fig. 2(b)) for joint segmentation and uncertainty estimation by fusing Monte Carlo sampling to better preserves

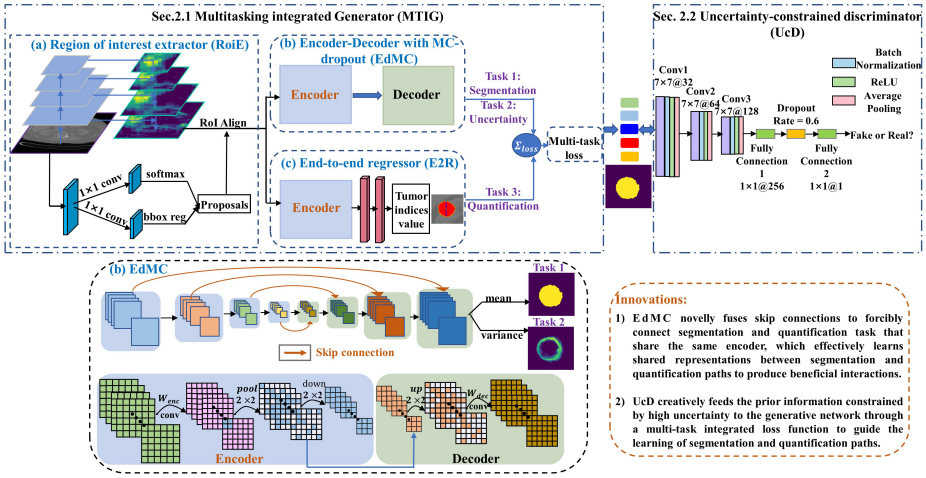

Fig. 2. Our proposed Mt-UcGAN achieves segmentation, quantification, and uncertainty estimation of renal tumors. An innovative adversarial mechanism of uncertainty constraints effectively integrates multiple tasks through joint learning and learns the prior information of uncertainty constraint feedback.

class boundary information, and a regressor that shares the same encoder with the encoder-decoder (see Fig. 2(c)) for the quantification of five tumor indices (i.e., the center point coordinates, diameter, circumference, and cross-sectional area) by fusing skip connections to interact with the segmentation network. 2) Uncertainty-constrained discriminator (Section 2.2) for guidance on the learning of segmentation and quantification network by feeding back the prior knowledge of high uncertainty to the generator to monitor and encourage the generative model to generate correct predictions.

2.1 Multitasking integrated generator (MtIG) for joint learning

The MtIG integrates region of interest extractor, encoder-decoder with MC-dropout and end-to-end regressor into the generator, which simultaneously implements pixel-level semantic segmentation, indices quantification, and uncertainty estimation of segmentation through joint learning.

Region of interest extractor (RoiE) connects hierarchical pyramid feature extraction network and region proposal network for extraction of the tumor regions of interest (see Fig. 2(a)). The hierarchical pyramid feature extraction network effectively detects early small renal tumor targets. This combines low-resolution but semantically strong features with high-resolution but semantically weak features through top-down paths and horizontal connections based on the principle of the pyramid structure. The result is high-level semantic information at all scales. The extraction of the region of interest reduces the amount of post-processing data, while eliminating some noise by determining the general

location of the tumor, reduces the time complexity of the network, and increases accuracy.

Encoder-decoder with MC-dropout (EdMC) novelly incorporates Monte-Carlo sampling for joint segmentation and uncertainty estimation of the renal tumor (see Fig. 2(b)). It includes a series of encoders and a corresponding set of decoders, followed by a per-pixel classifier. Each encoder consists of one or more non-linear convolutional layers with batch normalization and ReLU, followed by non-overlapping maximum pooling or subsampling. Each decoder contains multiple convolutional layers and then up-samples the sparse encoding due to the merging process using the largest pool index in the encoding sequence. Each encoder corresponds to a decoder by skip connections. This effectively preserves class boundary details and reduces the total number of model parameters. A dropout layer is then inserted after each encoder and each decoder unit. Multiple sampling is achieved through the dropout layer. The average of multiple samples is the final output corresponding to the image semantic segmentation, and the sample variance represents the uncertainty of the model prediction. The mask loss L_{m} are derived from the following formulas:

$$L_m\left(m_{it}, m_{ip}\right) = -\left(m_{ip}\log\left(m_{ip}\right) + \left(1 - m_{it}\right)\log\left(1 - m_{ip}\right)\right) \tag{1}$$

where the variable m_{it} represents the mask binary matrices from the prediction and m_{ip} represents ground-truth label.

End-to-end regressor (E_2R) that shares encoder with the segmentation network novelly merges skip connections to force learning of the shared representation of segmentation and quantification to produce beneficial interactions for the prediction of the tumor indices (i.e., the center point coordinates, diameter, circumference, and cross-sectional area) (see Fig. 2(c)), which reduces the interference of unified optimization of segmentation and quantification on segmentation. The error function is based on the difference between the predicted and actual values, and the mapping relationship is derived from the following formula:

$$L_{\mathrm{r}}\left(x_{i_i}, \mathrm{x}_{ip}\right) = \mathrm{smooth}_{L1}\left(v_{it} - v_{ip}\right), \mathrm{smooth}_{L1}(x) = \begin{cases} 0.5x^2 & \text{if } |x| < 1 \\ |x| - 5 & \text{otherwise} \end{cases} \tag{2}$$

Where x_{ip} variable represents the predicted value of five indices (i.e., the center point coordinates (X, Y), diameter (D), circumference (C), and cross-sectional area (S) of the tumor), and x_{it} represents the measured value of the real label.

The global loss function of multitasking integrated generator (MtIG) incorporating dual paths is defined as:

$$\begin{aligned} L_{MtIG}\left(m_{it}, m_{ip}, b_{it}, b_{ip}, v_{it}, v_{ip}\right) = & \underbrace{\gamma \frac{1}{N_{r2}} \sum_i p_{it} L_r\left(b_{ip}, b_{it}\right)}_{\text{Object Detection}} \\ & + \underbrace{\beta \frac{1}{N_{mask}} L_m\left(m_{it}, m_{ip}\right)}_{\text{Segmentation path}} + \underbrace{\delta \frac{1}{N_{r3}} \sum_i p_{it} L_r\left(v_{ip}, v_{it}\right)}_{\text{Quantification path}} \end{aligned} \tag{3}$$

where constant N represents the number of corresponding bounding boxes. These hyperparameters β, γ and δ are set to 0.2, 0.3 and 0.5 respectively according to experience and practice to balance the training losses of different tasks.

Summarized advantage: The multitasking integrated generator novelly merges skip connection and Monte Carlo sampling to represent different tasks as a unified framework, thereby generating beneficial interactions, reducing the interference of unified optimization of segmentation and quantification networks on segmentation.

2.2 Uncertainty-constrained discriminator (UcD) for adversarial guided learning

The UcD module monitors and encourages generative models to generate correct predictions through adversarial learning guided by the high uncertainty of the generative model (see Fig. 2). Under the adversarial mechanism, the UcD module receives prediction maps with high uncertainty from the generator or manual maps from ground truth as input and then outputs a single scalar indicating whether the input is from the generative network or ground truth. Then it feeds the prior information of uncertainty constraints to the generator through the multi-task comprehensive loss function to guide the learning of segmentation and quantification networks. When strong adversarial learning occurs, the discriminative network eagerly causes the generative model to look for mismatches in various high-order statistics between the predicted segmentation map and the ground truth. The hybrid loss function of Mt-UcGAN is defined as:

$$\begin{aligned} L_{Mt-UcGAN}\left(\theta_{\mathrm{s}}, \theta_{d}\right) = & \underbrace{\frac{1}{N_{\mathrm{m}}} \sum_{i} L_{MtIG}\left(\mathrm{m}_{it}, \mathrm{m}_{it}, \mathrm{m}_{ip}, \mathrm{b}_{it}, \mathrm{b}_{ip}, \mathrm{v}_{it}, \mathrm{v}_{ip}\right)}_{\text{Multitasking Integrated generator}} \\ & \underbrace{-\lambda\left[L_{UcD}\left(D\left(m_{it}\right), 1\right)+L_{UcD}\left(m_{ip}, 0\right)\right]}_{\text{Uncertainty-constrained Discriminator}} \end{aligned} \tag{4}$$

λ is set to one to maintain the balance of adversarial learning. The weighted two-class cross-entropy loss of UcD is defined as:

$$L_{UcD}\left(\mathrm{m}_{it}, UcD\left(\mathrm{m}_{it}\right)\right) = -\left[m_{it} \log UcD\left(m_{it}\right)+\left(1-m_{it}\right) \log\left(1-UcD\left(m_{it}\right)\right)\right] \tag{5}$$

where m_{it} is the input labels (fake maps are zeros and ground maps are ones), while $UcD\left(\mathrm{m}_{it}\right)$ are the single scalar of the output of the discriminative network.

Summarized advantage: The uncertainty-constrained discriminator creatively feeds the prior knowledge of prediction results with high uncertainty to the generative network to guide the learning of segmentation and quantification path.

3 Experiments and Results

The Mt-UcGAN demonstrates high segmentation performance with a pixel accuracy of 97.3%, high quantification performance with the R^2 coefficients of tumor circumference is 0.9513 and low uncertainty (see Fig. 3). Experimental results demonstrate the effectiveness of this method in segmentation, quantification, and uncertainty estimation of renal tumors on CT.

Dataset and Configuration. A total of 3000 2D axial slices composed of 113 subjects with renal tumors is selected as the experiment. Two radiologists with more than ten years of experience manually segmented and quantified renal tumors on CT images. If there are differences, a consensus must be reached between the two experts. Our deep learning model was implemented using TensorFlow 1.3.0, Keras 2.0.8 on an Ubuntu 16.04 machine, and was trained and tested on an NVIDIA Titan Xp 12GB GPU. All experiments were assessed with a 10-fold cross-validation test. Divide the data set into ten parts, taking nine of them as training data and one part as test data in turn. The average value of the accuracy of the ten results is used as an estimate of the accuracy of the algorithm. We alternately optimize the hybrid loss function of the segmentation network and the loss function of the discriminant network in the Mt-UcGAN. First, the parameters of the discriminant network are fixed to optimize the generation network, and then the discriminative network is optimized according to the updated parameters. It alternates until the network converges.

Accurate Segmentation. The experimental results show that Mt-UcGAN has high segmentation performance with a pixel accuracy of 97.3%, a dice coefficient of 92.1%, a sensitivity of 95.7%, a specificity of 93.4%, as shown in Table 2 and Table 3.

Precise Quantification. The proposed Mt-UcGAN has high quantitative performance as shown in Table 1. The R^2 coefficients predicted by our method for the five tumor indices are 0.9321 in X-coordinate of tumor center point, 0.9402 in Y-coordinate of tumor center point, 0.9289 in diameter, 0.9513 in circumference and 0.9485 in area. It shows that the values of the tumor indices predicted by our method are very close to the actual values, and the fitting effect is very well.

Table 1. Mt-UcGAN yielded higher quantitative performance on the five indexes of tumors. The R^2 coefficients are all close to 1.

Metrics	X-coordinate	Y-coordinate	Diameter(D)	Circumference(C)	Area(S)
R^2 coefficient	0.9321	0.9402	0.9289	0.9513	0.9485

Advantage of Mt-UcGANs architecture (Ablation study). Table 2 demonstrates that each of our technological innovations in Mt-UcGANs has effectively improved the accuracy of the renal tumor segmentation. The third row is about 8% higher than the second row in pixel accuracy, indicating that skip connection can significantly reduce the interference on segmentation caused by

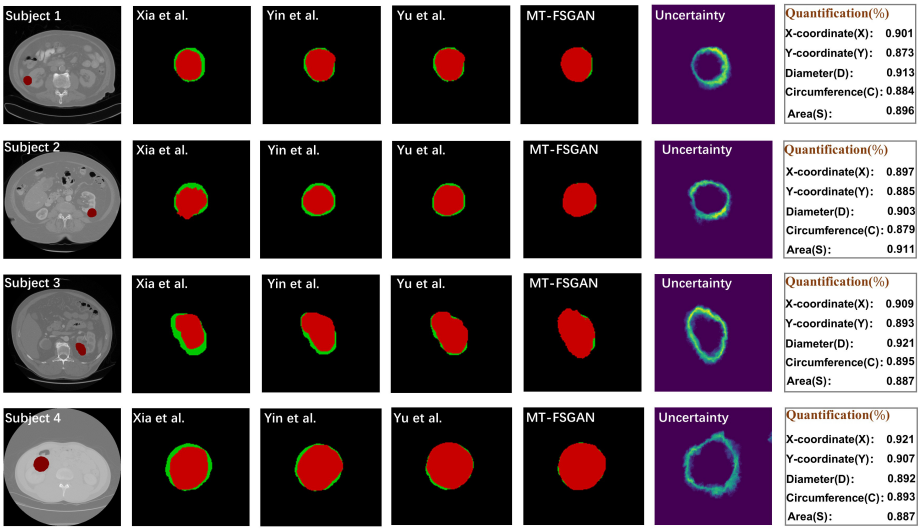

Fig. 3. The comparison of segmentation results between the proposed method and three typical deep learning networks indicates that the performance of the network is superior. The first column is Groundtruth, and the second to fifth columns are the latest deep learning methods [22–24] and our method for renal tumor lesion segmentation comparison. The last column is uncertainty estimation of our segmentation results.

the unified optimization of segmentation and quantification. The fourth row is about 5% higher than the third row in pixel accuracy, indicating that Monte Carlo sampling can improve the accuracy of the network. The fifth row is about 5% higher than the fourth row in pixel accuracy, indicating that the constraint of uncertainty can improve the accuracy of the network.

Table 2. Each of our technological innovations in Mt-UcGANs effectively improved the segmentation accuracy of network.

Method	Pixel accuracy	Dice coefficient	Specificity	Sensitivity
Ed	83.5%	79.6%	80.7%	81.8%
Ed+E_2R	74.3%	71.9%	73.5%	74.4%
Ed+E_2R+skip	87.5%	82.6%	83.7%	84.8%
EdMC+E_2R+skip	92.3%	87.1%	88.6%	89.1%
EdMC+E_2R+skip+UcD	**97.3%**	**92.1%**	**95.7%**	**93.4%**

Comparison with state-of-the-art methods. This paper tracks a comparison of segmentation performance among the proposed method and state-of-the-art method [22–24] by pixel accuracy, dice coefficient, specificity, sensitivity as shown in Table 3. The segmentation result of our proposed method is closest to ground truth compared with the state-of-art deep learning methods (see Fig.

3). To directly evaluate the quality of the segmentation process, Figure 3 shows the cross-sectional images from the same cube.

Table 3. Mt-UcGAN yielded higher performance than state-of-art segmentation methods on renal tumors.

Method	Pixel accuracy	Dice coefficient	Specificity	Sensitivity
Proposed method	**97.3%**	**92.1%**	**95.7%**	**93.4%**
Yin, Kevin, et al.[22]	92.1%	79.6%	86.7%	83.4%
Xia, Kai-jian, et al.[23]	89.4%	83.8%	81.1%	85.4%
Yu, Qian, et al.[24]	87.7%	80.4%	83.4%	82.2%

4 Conclusion

For the first time, a multi-task uncertainty-constrained generative adversarial network (Mt-UcGAN) was proposed for joint segmentation, quantification, and uncertainty estimation of renal tumors. We creatively proposed an adversarial mechanism with uncertainty constraints. Experiment results demonstrate that Mt-UcGAN can aid in the clinical diagnosis of tumor assessments. And it can also provide clinicians with feedback on the reliability of the results, which helps doctors to conduct subsequent visual inspections and revisions on the results to further improve the accuracy of the diagnosis.

References

1. Mehrazin, R., Palazzi, K.L., Kopp, R.P., Colangelo, C.J., Stroup, S.P., Masterson,J.H., Liss, M.A., Cohen, S.A., Jabaji, R., Park, S.K., et al.: Impact of tumour morphology on renal function decline after partial nephrectomy. BJU international **111**(8), E374–E382 (2013)
2. Greene, F. L., Balch, C. M., Fleming, I. D., Fritz, A., Haller, D. G., Morrow,M., Page, D. L.: AJCC cancer staging handbook: TNM classification of malignant tumors. Springer Science Business Media (2002)
3. Spaliviero, M., Poon, B.Y., Aras, O., Di Paolo, P.L., Guglielmetti, G.B., Coleman, C.Z., Karlo, C.A., Bernstein, M.L., Sjoberg, D.D., Russo, P., et al.: Interobserver variability of RENAL, PADUA, and centrality index nephrometry score systems. World journal of urology **33**(6), 853–858 (2015)
4. Kutikov, A., Uzzo, R.G.: The renal nephrometry score: a comprehensive standardized system for quantitating renal tumor size, location and depth. The Journal of urology **182**(3), 844–853 (2009)
5. Ficarra, V., Novara, G., Secco, S., Macchi, V., Porzionato, A., De Caro, R., Artibani, W.: Preoperative aspects and dimensions used for an anatomical (PADUA) classification of renal tumours in patients who are candidates for nephron-sparing surgery. European urology **56**(5), 786–793 (2009)

6. Taha, A., Lo, P., Li, J., Zhao, T.: Kid-net: convolution networks for kidney vessels segmentation from ct-volumes. In: International Conference on Medical Image Computing and Computer-Assisted Intervention. pp. 463–471. Springer (2018)
7. Yang, G., Li, G., Pan, T., Kong, Y., Wu, J., Shu, H., Luo, L., Dillenseger, J.-L.,Coatrieux, J.-L., Tang, L., et al.: Automatic segmentation of kidney and renal tumor in ct images based on 3d fully convolutional neural network with pyramid pooling module. In: 2018 24th International Conference on Pattern Recognition (ICPR). IEEE, pp. 3790–3795(2018)
8. Edge, S.B., Byrd, D.R., Carducci, M.A., Compton, C.C., Fritz, A., Greene, F.,et al.: AJCC cancer staging manual, vol. 649. Springer New York (2010)
9. Afshin, M., Ayed, I. B., Islam, A., Goela, A., Peters, T. M., Li, S.: Global assessment of cardiac function using image statistics in mri. In: International Conference on Medical Image Computing and Computer-Assisted Interven-tion. Springer, pp. 535–543 (2012)
10. Zhen, X., Wang, Z., Yu, M., Li, S.: Supervised descriptor learning formulti-output regression. In: Proceedings of the IEEE conference on computervision and pattern recognition. pp. 1211–1218 (2015)
11. Zhen, X., Zhang, H., Islam, A., Bhaduri, M., Chan, I., Li, S.: Directand simultaneous estimation of cardiac four chamber volumes by multioutput sparse regression. Medical image analysis **36**, 184–196 (2017)
12. Wu, H., Bailey, C., Rasoulinejad, P., Li, S.: Automatic landmark esti-mation for adolescent idiopathic scoliosis assessment using boostnet. In: In-ternational Conference on Medical Image Computing and Computer-AssistedIntervention. Springer, pp. 127–135 (2017)
13. Sun, H., Zhen, X., Bailey, C., Rasoulinejad, P., Yin, Y., Li, S.: Direct esti-mation of spinal cobb angles by structured multi-output regression. In: Inter-national Conference on Information Processing in Medical Imaging. Springer, pp. 529–540 (2017)
14. Zhen, X., Yu, M., Islam, A., Bhaduri, M., Chan, I., Li, S.: Descriptor learning via supervised manifold regularization for multioutput regression.IEEE transactions on neural networks and learning systems **28** (9), 2035–2047 (2016)
15. Bray, F., Ferlay, J., Soerjomataram, I., Siegel, R. L., Torre, L. A., Jemal, A.: Global cancer statistics 2018: Globocan estimates of incidence and mortality worldwide for 36 cancers in 185 countries. CA: a cancer journal for clinicians **68** (6), 394–424 (2018)
16. Xu, C., Howey, J., Ohorodnyk, P., Roth, M., Zhang, H., Li, S.: Segmentation and quantification of infarction without contrast agents via spatio temporal generative adversarial learning. Medical Image Analysis p. 101568 (2019)
17. Luo, G., Dong, S., Wang, W., Wang, K., Cao, S., Tam, C., Zhang, H., Howey, J., Ohorodnyk, P., Li, S.: Commensal correlation network between segmentation and direct area estimation for bi-ventricle quantification. Medical image analysis p.101591 (2019)
18. D, Yanan Ruan A , et al.: MB-FSGAN: Joint segmentation and quantification of kidney tumor on CT by the multi-branch feature sharing generative adversarial network. Medical Image Analysis (2020)
19. Jungo, A., Reyes, M.: Assessing reliability and challenges of uncertainty estimations for medical image segmentation. In: International Conference on Medical Image Computing and Computer-Assisted Intervention. pp. 48–56. Springer (2019)
20. Raghu, M., Blumer, K., Sayres, R., Obermeyer, Z., Kleinberg, R., Mullainathan,S., Kleinberg, J.: Direct uncertainty prediction for medical second opinions. arXiv preprint arXiv:1807.01771 (2018)

21. Wang, G., Li, W., Aertsen, M., Deprest, J., Ourselin, S., Vercauteren, T.: Aleatoric uncertainty estimation with test-time augmentation for medical image segmentation with convolutional neural networks. Neurocomputing **338**, 34–45 (2019)
22. Xia, K.j., Yin, H.s., Zhang, Y.d.: Deep semantic segmentation of kidney and space-occupying lesion area based on SCNN and ResNet models combined with SIFT-flow algorithm. Journal of medical systems **43**(1), 2 (2019)
23. Yin, K., Liu, C., Bardis, M., Martin, J., Liu, H., Ushinsky, A., Glavis-Bloom, J.,Chantaduly, C., Chow, D.S., Houshyar, R., et al.: Deep learning segmentation of kidneys with renal cell carcinoma. Journal of Clinical Oncology **37**, e16098-e16098 (2019)
24. Yu, Q., Shi, Y., Sun, J., Gao, Y., Zhu, J., Dai, Y.: Crossbar-net: A novel convolutional neural network for kidney tumor segmentation in ct images. IEEE transactions on image processing **28**(8), 4060-4074 (2019)